ACS APPLIED MATERIALS & INTERFACES

Research Article

www.acsami.org

GaN as an Interfacial Passivation Layer: Tuning Band Offset and Removing Fermi Level Pinning for III−V MOS Devices

Zhaofu Zhang,[†] Ruyue Cao,[†] Changhong Wang,[†] Hao-Bo Li,[†] Hong Dong,[†] Wei-hua Wang,[†] Feng Lu,[†] Yahui Cheng,[†] Xinjian Xie,[‡] Hui Liu,[†] Kyeongjae Cho,[§] Robert Wallace,[§] and Weichao Wang*,[†,§]

[†]College of Electronic Information and Optical Engineering, Nankai University, 300071 Tianjin, P. R. China

[‡]College of Materials Science, Hebei Technology University, 300401 Tianjin, P. R. China

[§]Department of Materials Science & Engineering, The University of Texas at Dallas, Richardson, Texas 75080, United States

Supporting Information

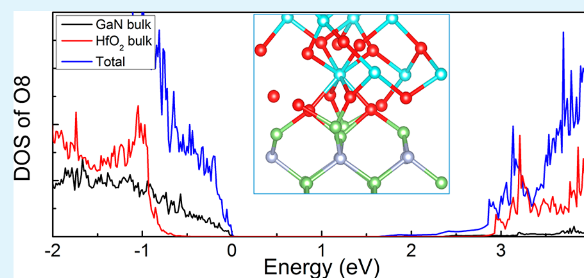

ABSTRACT: The use of an interfacial passivation layer is one important strategy for achieving a high quality interface between high-k and III−V materials integrated into high-mobility metal−oxide−semiconductor field-effect transistor (MOSFET) devices. Here, we propose gallium nitride (GaN) as the interfacial layer between III−V materials and hafnium oxide (HfO_2). Utilizing first-principles calculations, we explore the structural and electronic properties of the GaN/HfO_2 interface with respect to the interfacial oxygen contents. In the O-rich condition, an O8 interface (eight oxygen atoms at the interface, corresponding to 100% oxygen concentration) displays the most stability. By reducing the interfacial O concentration from 100 to 25%, we find that the interface formation energy increases; when sublayer oxygen vacancies exist, the interface becomes even less stable compared with O8. The band offset is also observed to be highly dependent on the interfacial oxygen concentration. Further analysis of the electronic structure shows that no interface states are present at the O8 interface. These findings indicate that the O8 interface serves as a promising candidate for high quality III−V MOS devices. Moreover, interfacial states are present when such interfacial oxygen is partially removed. The interface states, leading to Fermi level pinning, originate from unsaturated interfacial Ga atoms.

KEYWORDS: *first-principles study, GaN/HfO2 interface, interfacial formation energy, band offsets, Fermi level pinning*

1. INTRODUCTION

With the continued downscaling in the dimensions of complementary metal−oxide−semiconductor (CMOS) transistors, III−V compound semiconductors have the potential to be implemented in future CMOS devices as channel materials, among which $Ga_xIn_{1-x}As$ ($0 \leq x \leq 0.47$) with higher electron mobility and breakdown voltage compared to those of silicon is the most promising candidate.[1−3] It is known that current CMOS technology requires applying deposited high-k dielectrics, (e.g., hafnium oxide (HfO_2)) as the gate dielectric.[4,5] However, the typical gallium arsenide (GaAs) channel and high-k gate oxide interface have been shown to have poor properties leading to many problems, such as low electron mobility, Fermi level pinning, and unstable device operations.[6−11] One solution to remove the gap states of the $Ga_xIn_{1-x}As/HfO_2$ interface is to introduce an interlayer between the channel material and the high-k oxide.[12,13]

Similar to GaAs, cubic gallium nitride (GaN) also belongs to the III−V compound family and shares the same structural symmetry, and it is expected to readily achieve a high quality $Ga_xIn_{1-x}As$/GaN interface.[14−16] On the other hand, the GaN sandwich layer physically enlarges the distance between $Ga_xIn_{1-x}As$ and high-k dielectrics, and the remote phonon scattering effect on the carriers is reduced.[17] Besides, nitrogen passivation has been proven to be effective in a GaAs/Al_2O_3 interface.[18] Thus, we mainly focus on the interface between cubic GaN/high-k oxides in this study. Recently, a thermal stability study of the $Ga_xIn_{1-x}As$/high-k interface shows that electrical performance degrades concurrent with indium out diffusion through high-k oxides as post deposition annealing is applied.[19,20] Utilization of a GaN interface layer is one way to passivate $Ga_xIn_{1-x}As$ from a stability perspective upon being subjected to a post deposition annealing process.[21−25]

To develop a high quality interface for MOS applications, three aspects should be addressed: interface stability, useful band offsets, and mitigation of interfacial gap states. Experimentally, several efforts over the past decade have addressed the GaN/HfO_2 interface. In addition, experimental data about Fermi level pinning on the cubic GaN surface motivates this study.[26] Hong et al. found that GaN films grown on (100) GaAs substrates by metalorganic chemical vapor deposition (MOCVD) have (200) cubic or (111) cubic/(002) hexagonal phases.[21] Nemanich et al. demonstrated that valence band offsets could be tuned by annealing conditions by up to

Received: October 21, 2014
Accepted: February 2, 2015
Published: February 2, 2015

ACS Publications © 2015 American Chemical Society

DOI: 10.1021/am507287f
ACS Appl. Mater. Interfaces 2015, 7, 5141−5149

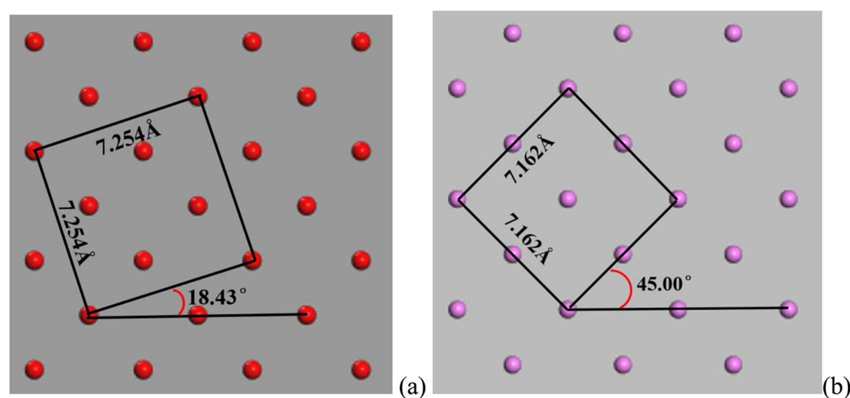

Figure 1. (a) Ga monolayer of the GaN (001) surface and (b) Hf monolayer of the HfO_2 (001) surface. Red atoms are Ga, and purple atoms are Hf.

~0.4 eV.[27] The density of interface states, which can result in Fermi level pinning, is another important factor that impacts the interface quality.[28,29] Guo et al. claimed improvement to $GaAs/Al_2O_3$ interface quality by nitridation of the GaAs surface prior to HfO_2 deposition using first-principles calculation.[30] Recent work by Stemmer on InGaAs (100) and InAs (100) shows that remote plasma nitridation plus atomic layer deposition (ALD) is also beneficial.[31,32] However, the detailed interfacial chemistry is not yet clearly understood. Despite tremendous efforts dedicated to investigating properties of the GaN/HfO_2 interface, the fundamental question of whether the cubic GaN layer is useful in passivating the III−V/HfO_2 interface has not been addressed.[21−25]

In this work, we present a theoretical investigation of the atomic and electronic properties for cubic GaN/HfO_2 interfaces at different interfacial oxygen concentrations. Interfacial oxygen atoms were gradually removed to mimic the influence of ambient oxygen pressure on interface quality during the HfO_2 growth process. Oxygen atoms from different sublayers were removed to explore oxygen vacancy conditions. Interface formation energy was studied to determine the preferable interface structure under specific chemical environments. Furthermore, we explored the electronic structure and elucidated the impact of various interfacial oxygen content models on the interface as well as the origin of the interface states through local density of states (LDOS) and Bader charge analysis. Finally, on the basis of our calculated results of interface stability, band offsets, and suppression of the gap states, we find that the cubic GaN O8 interface is strongly superior to the others tested in serving as a passivation layer for the III−V/HfO_2 interface.

2. THEORETICAL BASIS

All of the calculation work was done within the density functional theory (DFT)[33,34] with the Perdew, Burke, and Ernzerhof (PBE)[35] version of the generalized gradient approximation (GGA), as implemented in the plane-wave basis code Vienna ab-initio simulation package (VASP).[36,37] The projector augmented wave (PAW)[38] method was applied to describe the pseudopotential. An energy cutoff of 400 eV and a $6 \times 6 \times 1$ k-point gamma-centered mesh were used for the convergence test. The convergence criterion was chosen as 10^{-3} eV between two ionic steps in the atomic structure optimization.

We used a slab model of cubic HfO_2 (001) and GaN (001) surfaces with Ga−O bonding at the interface, which was observed to be stable at the experimental interface terminated with Ga−O bonds.[39,40] Worth noting is that HfO_2 exists in monoclinic, tetragonal, and cubic phases, and GaN in wurtzite and cubic phases; the cubic phase was chosen in our calculations because it is the simplest both structurally and computationally.[41] Moreover, the analysis conclusion could still be useful for other phases because they share the same valence. If two slabs simply combine without rotating one slab to comprise the strain, an extremely thin cubic GaN would be needed in practice to serve as an effective buffer layer between GaAs and HfO_2. For GaAs-based structures (i.e., HfO_2/GaN/GaAs), we employ the rotation strategy to avoid lattice mismatch at the interfaces. The HfO_2 surface was rotated clockwise by 26.57° to match the GaN (001) surface (Figure 1), and the lattice mismatch was only 1.28%, which means that strain exists within the unit cell not among the supercells of the HfO_2/GaN interface (see rotation details of the GaN/GaAs interface in Figure S1 in the Supporting Information (SI)). Additionally, prior to interface explorations, GaN (001) surface reconstructions and correlated electronic structures were calculated and are listed in Figures S2 and S3 in the SI. On the basis of the surface study, we find significant surface states that lead to Fermi level pinning. In the HfO_2/GaN model, a 10 Å vacuum region was adopted to avoid interaction between the slab and its images. The bottom atomic layer of the slab (N) was passivated by pseudohydrogen (with 0.75 valence electron) to saturate dangling bonds. Meanwhile, for the top atomic layer (HfO_2) of the slab, half of the oxygen atoms were removed to generate an insulating HfO_2 surface without surface states. Thus, the passivation of the top (HfO_2) and bottom (GaN) surfaces guarantees that all of the gap states originate from atomic interactions at the interface. The GaN slab contains 8 layers of GaN (40 Ga and 40 N atoms), whereas the HfO_2 slab comprises 5 layers of Hf (20 Hf atoms) and 6 layers of O (44 O atoms). Layer-thickness testing details can be found in Figure S4 in the SI.

It is known that DFT cannot locate the global energy minimum. To solve this problem, the HfO_2 slab was moved in the x, y, and z directions relative to the GaN slab. After the HfO_2 slab movements, we obtained an initial structure with energy minima along the three directions. Subsequently, the initial structure was optimized using the conjugate gradient (CG)[42] optimization method with only the bottom N and pseudohydrogen layers fixed. The details of this analysis are described in Figure S5 in the SI.

3. RESULTS AND DISCUSSIONS

3.1. Interfacial Bonding. Interfacial bonding at the GaN/HfO_2 interface is more complicated than that at a traditional Si/SiO_2 interface (where only covalent Si−O bonds exist) owing to the coexistence of covalent and ionic bonds at the GaN/HfO_2 interface. Multiple atomic terminations, such as Ga−O, N−O, Ga−Hf, and N−Hf bonds, might form at the interface. These various bonds could lead to interfacial gap states that pin the Fermi level. Unlike Si/SiO_2 in which each interfacial Si dangling bond has one electron, unsaturated Si bonds could be readily passivated by O or H.[43−45] For GaN/HfO_2, each interfacial N or Ga dangling bond has 1.25 or 0.75 electrons, respectively, which makes charge compensation difficult. Among all of the various possible bondings at the GaN/HfO_2 interface, Ga−O shows the most stability due to it having the largest electronegativity (EN) difference.[46] Experimental results also prove this to be true.[38,39] In the following context, we primarily focus on the Ga−O bond, which is in proximity of HfO_2 at the interface.

The fully oxidized interface slab model explored here contains eight oxygen atoms at the interface, labeled as O8. The interfacial oxygen atoms are gradually removed to mimic the influence of ambient oxygen pressure on the interface quality during the HfO_2 growth process.[47] Different models are similarly labeled by their interfacial oxygen content, such as O7, O6, and so forth. On the basis of the O8 interface, one oxygen atom in the second, third, or fourth layer is also removed (labeled as Vo_L2, Vo_L3, and Vo_L4, respectively) to simulate the presence of oxygen vacancies. For each sublayer oxygen vacancy, all possible locations were considered, but only the interface with the lowest energy is presented in this work.

The side view structures of GaN/HfO_2 slabs with various interfacial oxygen contents (O8−O2) are presented in Figure 2. Realistically, it is not necessary to test further oxygen removal because not only is it challenging to obtain such O-poor experimental conditions but the O-poor interfaces would show metallic behaviors, which do not meet the requirements for high quality interfaces in high mobility MOSFET devices. Thus, only the O8−O2 interfaces are presented here.

Figure 3 shows the side view of the ideal GaN/HfO_2 O8 interfaces with oxygen vacancies Vo_L2−Vo_L4.

At the O8 interface (see Figure 2(a)), the interfacial Ga atoms move toward the oxygen atoms. The optimized Ga−O bond length is 1.97 ± 0.08 Å, which is in good agreement with the experimental result of Ga_2O_3 bulk (2.01 ± 0.10 Å).[48,49] We observe that one dangling bond exists on the interfacial Ga atoms, which likely contributes to the interface state. Starting with the O8 model, we remove one interfacial oxygen atom to generate interface O7. Eight possible interfacial oxygen atom locations are tested one by one to find the one that is the most stable. The same procedure is then applied for the O6 interface generated from the O7 interface. This process is repeated for interfaces O5, O4, O3, O2, as well as the original O8 with different vacancies.

Table 1 shows the bond lengths of interfacial Ga−O and Ga−N bonds in the various models. It is found that with decreasing interfacial oxygen content that the interfacial Ga−O bond lengths gradually approach the Ga−O bond length in bulk Ga_2O_3, whereas the Ga−N lengths at the interface differ slightly from the bulk GaN value. Table 1 also indicates that the interfacial bonding strength declines as the oxygen content is reduced.

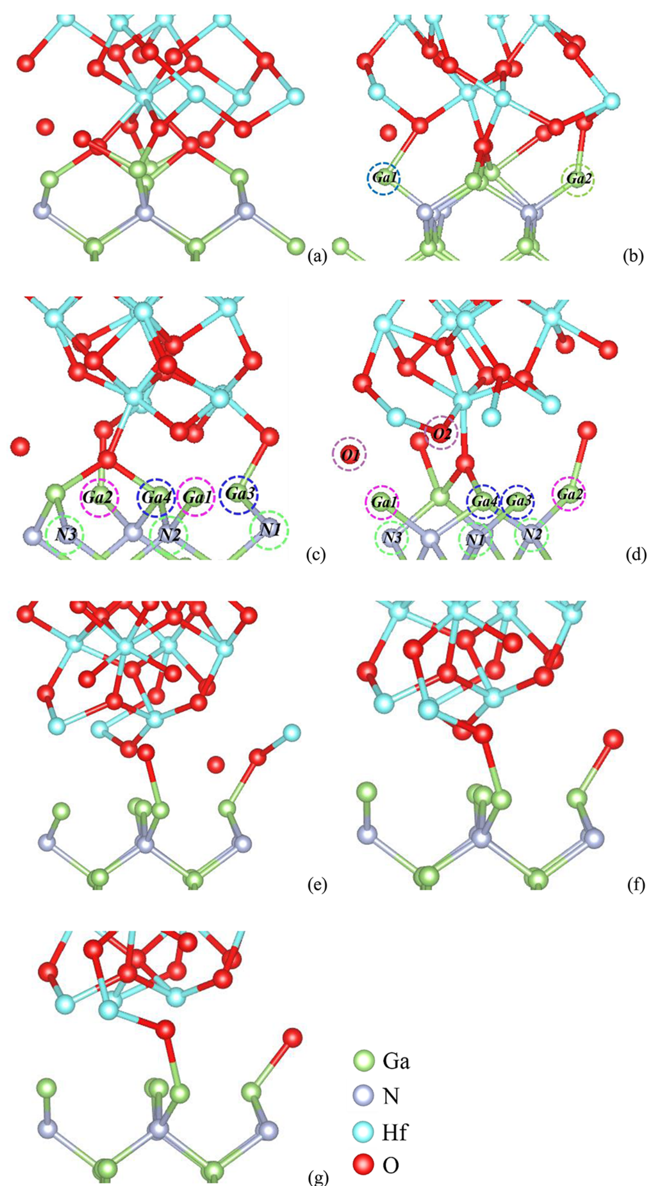

Figure 2. (a−g) Side view of GaN/HfO_2 interfaces from O8 to O2, respectively.The Ga, N, Hf, and O atoms are depicted by green, blue, light blue, and red balls, respectively. Atoms contributing to interface states are highlighted by dashed circles.

3.2. Interface Stability. Experimentally, it is challenging to grow oxides on a GaN surface due to the inertness of the GaN (001) surface.[39,40] Here, we explore interface stability through the interface formation energy. The interface formation energy of a repeated slab model can be expressed as[50]

$$E_{\text{form}} = \frac{E_{\text{total}} - [xE_{\text{HfO}_2} + yE_{\text{Ga}} + z(E_{\text{GaN}} - E_{\text{Ga}}) \pm l\mu_{\text{O}}]}{A} \quad (1)$$

where x, y, and z are the number of HfO_2 cells, Ga atoms, and N atoms, respectively, l is the excess/deficient oxygen atoms (determined by the relative number of Hf and O atoms), parameter A represents the supercell area ($A = a \times b$, where a and b are the lattice constants), E_{total} is the total DFT energy of the interface supercell, E_{Ga} is the atomic energy of bulk Ga, and E_{HfO_2} and E_{GaN} are the total energy per unit cell in the bulk materials. The reference energy for pseudohydrogen is constant

DOI: 10.1021/am507287f
ACS Appl. Mater. Interfaces 2015, 7, 5141−5149

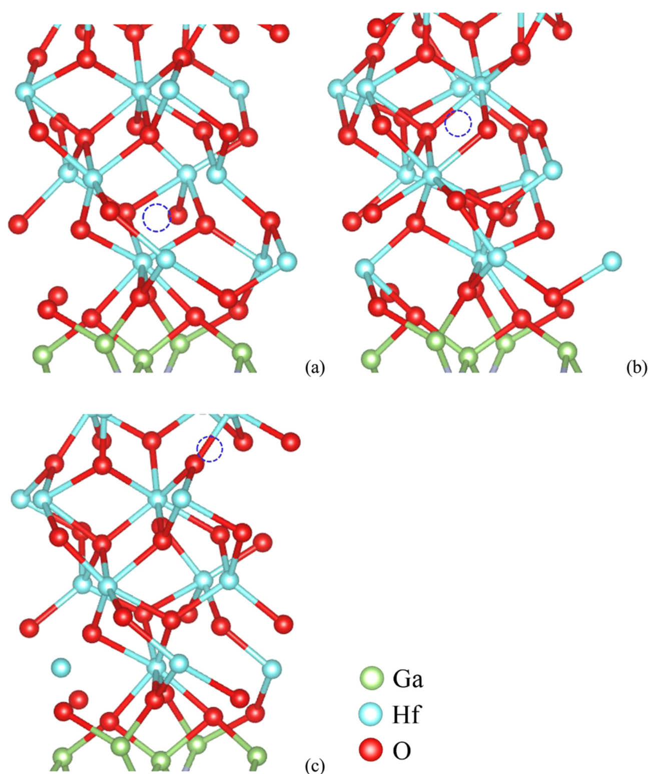

Figure 3. (a−c) Side view of GaN/HfO_2 interfaces with oxygen vacancy for Vo_L2−Vo_L4, respspectively. The Ga, N, Hf, and O atoms are depicted by green, blue, light blue, and red balls. The vacant sites are highlighted by a dashed circle.

Table 1. Bond Lengths of Interfacial Ga−O and Ga−N Bonds

interface model	Ga−O bond (Å)	Ga−N bond (Å)
O8	1.97 ± 0.08	1.991
O7	1.99 ± 0.22	1.992
O6	1.97 ± 0.02	1.994
O5	1.97 ± 0.04	1.996
O4	2.00 ± 0.02	2.004
O3	2.01 ± 0.02	2.015
O2	2.00	2.024
Vo_L2	1.97 ± 0.08	1.991
Vo_L3	2.00 ± 0.09	1.973
Vo_L4	1.99 ± 0.09	1.975
experimental	2.01 ± 0.10[a]	1.987[b]

[a]Ga_2O_3 bulk. [b]GaN bulk.

and thus not included in this equation. A more stable interface presents a lower formation energy. On the basis of our previous work,[47] we conclude that the range of oxygen chemical potentials μ_O is constrained within

$$\frac{1}{2}(E_{O_2} + \text{Hf}) \leq \mu_O \leq \frac{1}{2}E_{O_2} \quad (2)$$

Once the range for the chemical potential of oxygen is determined, we can express the interface formation energy as a function of μ_O (with only μ_O unknown and the other parameters as constants). We define the maximum of μ_O as 0 eV, representing the vacuum chemical potential. Thus, the μ_O range is

$$-5.38 \text{ eV} < \mu_O < 0 \text{ eV} \quad (3)$$

Equation 3 indicates that the chemical potential of oxygen ranges from 0 eV for O-rich conditions to −5.38 eV for O-poor conditions. Figure 4 shows the interface formation energies of

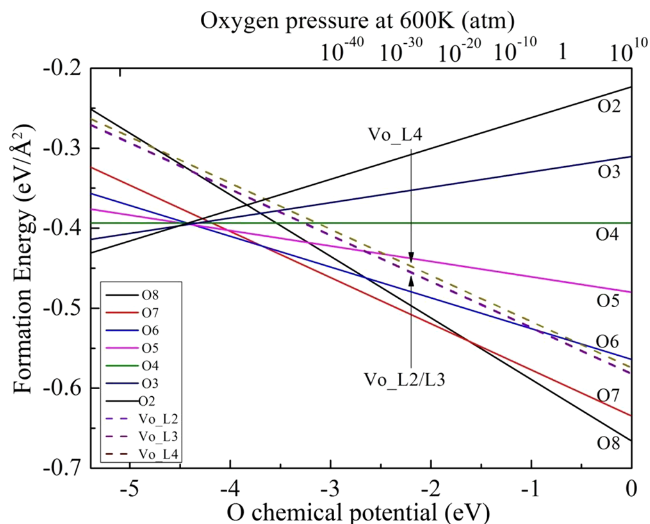

Figure 4. Interface formation energies of various structures as a function of oxygen chemical potential.

various structures as a function of oxygen chemical potential. The contribution of pseudohydrogen is neglected in eq 1 because it is the same for each model.

In the extremely O-rich environment (μ_O = 0 eV), the formation energy of O8 and O2 are located at the bottom (−0.67 eV) and top (−0.22 eV) in Figure 4, respectively, which indicates that the O8 model shows the most stability, whereas the O2 model is least stable. By reducing the interfacial O content from 100 to 25% (i.e., varying the oxygen partial pressure during oxide growth), we find that the more stable interfaces within the O chemical potentials from −5 to 0 eV are O8, O7, O6, and O2. Within the range between −1.58 and 0 eV of μ_O, the formation energy of O8 increases rapidly with the largest slope; meanwhile, O7 is the most stable in the range −3.68 eV < μ_O < −1.58 eV. Decreasing μ_O further results in O6 replacing O7 as the most stabile. In the Hf-rich condition, O2 is the most stable, and a metallic interface forms, which is not an optimal oxygen growth condition.

Interfaces become less stable when sublayer vacancy of oxygen (VO) exists relative to O8. The stabilities of vacant systems are almost the same in Vo_L2 and Vo_L3 but become more unstable when VO increases relative to Vo_L3. Thus, we conclude that introducing oxygen vacancy into HfO_2 could cause interface instability.

To combine our theoretical results with the experimental ALD growth condition of HfO_2, we take the ambient oxygen atmosphere and temperature into consideration. To grow HfO_2 on hexagonal GaN by ALD, 600 K is typically applied.[39] In this work, similar deposition conditions are assumed for cubic GaN as those applied for hexagonal GaN. We know that oxygen partial pressure is related to its chemical potential, formulated as[51]

$$\mu_O(T, P) = \mu_O(T, P^0) + \frac{1}{2}KT \ln \frac{P}{P^0} \quad (4)$$

where P and P^0 indicate the pressure at temperature T and 1 atm pressure, respectively. Figure 4 shows the dependence of

DOI: 10.1021/am507287f
ACS Appl. Mater. Interfaces 2015, 7, 5141−5149

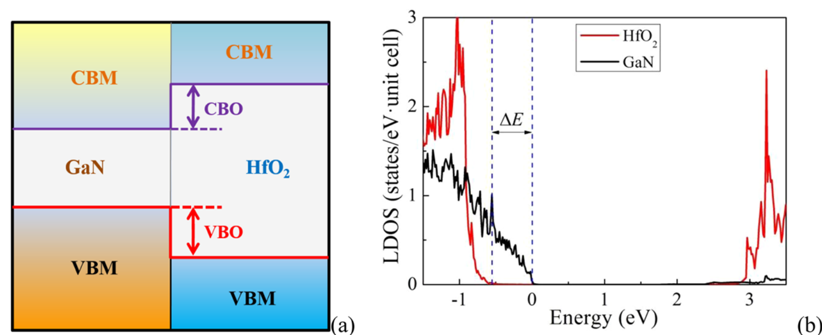

Figure 5. (a) Schematic diagram of GaN/HfO_2 interface energy band and (b) LDOS of the bulk layer GaN and HfO_2 atoms.

interface stability on the O_2 partial pressure at 600 K. We conclude that any ambient O_2 pressure larger than 1 atm causes a highly oxygen-terminated interface (almost O8). Oxygen-poor metallic interfaces are expected to lead to Fermi level pinning in an electronic device, causing a negative effect on the field effect operation characteristics.[52]

It has to be noted that the discussion above is based solely on thermodynamic arguments on interfaces formed from bulk-terminated surfaces without kinetic effects. However, these results provide important trends on improving interface quality by controlling growth conditions.

3.3. Band Offsets. To obtain a high quality interface, the band offsets (BOs) between GaN and HfO_2 must be considered. When two different materials contact, discontinuous offsets occur at the conduction band minimum (CBM) and the valence band maximum (VBM), which are called conduction band offset (CBO) and valence band offset (VBO), respectively.[52] The band offsets control charge transfer at the interface; in the absence of charge transfer, they are regulated by Anderson's electron affinities rules (EAR). Both charge transfer and electron affinity are strongly effected by interfacial oxygen concentrations. In other words, varying the interfacial oxygen content could in principle be used to tune electron transfer and electron affinity at the interface. Essentially, the BOs should be engineered by the interfacial oxygen content, which is controlled by the oxygen partial pressure during oxide growth.

In the present theoretical work, the band offsets are obtained according to the local density of states scheme[53] as shown in Figure 5. The schematic diagram of band structure is presented in Figure 5(a), where the CBM and VBM are highlighted. The band gaps assumed are from the experimentally determined values (3.2 eV for GaN[54,55] and 5.6 eV for HfO_2[4,13]). In this diagram, GaN's CBM should be lower than that of HfO_2 because otherwise electrons could not be effectively confined in the side of the III−V materials. In Figure 5(b), we present how to derive the BOs through the LDOS method. The LDOS of atoms in the GaN and HfO_2 that are sufficiently distant from the interface and show bulk behaviors are calculated, and the energy differences between their VB maxima (i.e., VBOs) are determined. As is known, DFT cannot accurately describe the excited states; the CBOs described here are thus derived by using the experimental values for the band gaps of GaN and HfO_2. The calculated BOs are shown in Table 2.

In practice, an effective MOS device requires BOs over 1 eV to confine the electron in the channel material region. An interface with small band offset (<1 eV) could cause charge at the interface tunneling and thus substantial leakage of current. As the VBM of HfO_2 is dominated mainly by oxygen 2*p* orbitals, the interfacial oxygen content has a large impact on the VBM of metal oxides but not on that of GaN. Thus, the VBOs of the GaN/HfO_2 interfaces are changed significantly by the interfacial O content. Electrons accumulate within valence bands, which means that upon decreasing the interfacial O content, increased VBOs are attributed to downward movement of the HfO_2 VB edge due to reduced electronegativity of the total interfacial oxygen compared to that of O8. This means that a reduced O 2*p* distribution at the VBM lowers the VB edge, resulting in less electronegativity. Table 2 shows that VBO of O8 is 0.51 eV. With the interfacial oxygen content decreased from O8 to O2, the VBO increases from 0.51 to 1.97 eV, and the CBO decreases from 1.89 to 0.43 eV, respectively. Furthermore, BOs of O6 and O5 are all >1 eV. As for O3 and O2, a small CBO will cause charge transfer and uncontrollable tunneling at the CBM, leading to poor device quality. The strong dependence of BO on interfacial content indicates that BO variation could be achieved by varying the ambient oxygen pressure during HfO_2 growth.

Table 2. Band Offsets of All Interface Models

model	VBO (eV)	CBO (eV)
O8	0.51	1.89
O7	0.82	1.58
O6	1.23	1.17
O5	1.30	1.10
O4	1.47	0.93
O3	1.85	0.55
O2	1.97	0.43
V_O_L2	0.98	1.42
V_O_L3	0.99	1.41
V_O_L4	0.97	1.43

For the most stable interface (O8), the CBO is 1.89 eV. Combined with the CBO of $GaAs/HfO_2$,[47] we propose the following scenario on how $GaAs/GaN/HfO_2$ band offsets align (Figure 6). In this schematic diagram, the carrier electron is confined in the GaAs region (channel material) due to its lower CBM than that of GaN. Therefore, from the BO point of view, GaN is a promising candidate as an interlayer for the $GaAs/HfO_2$ interface. Of course, different oxide growth conditions might lead to different BO line-ups, which could influence the confinement of the carrier electrons.[27,56]

It is worthwhile to point out that there are two ways to determine the band offsets between two semiconductors/insulators: LDOS and the average potentials line-up methods.[57,58] In principle, these two methods should provide the same outcomes with minor differences. In this work, the LDOS method was adopted.

DOI: 10.1021/am507287f
ACS Appl. Mater. Interfaces 2015, 7, 5141−5149

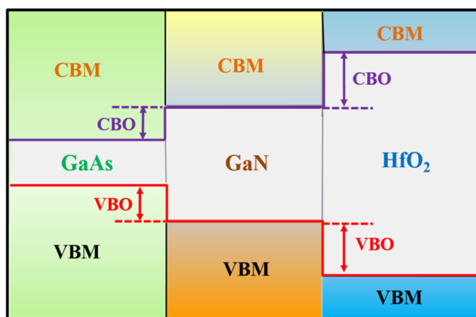

Figure 6. Schematic diagram of GaAs/GaN/HfO_2 interface band.

3.4. Interface States.

If significant interface states dominate within the GaN band gap, Fermi level pinning occurs and causes the gate voltage field control of the transistor channel to be compromised. This is because the regular operation of MOSFET requires field control in which the Fermi level can be swept to vary the carrier density in the MOS channel.[59] The density of states (DOSs) of various interface models are displayed in Figure 7 (O3−O8) and Figure 8 (Vo_L2−Vo_L4), where the VBMs are aligned at 0, making it easier to distinguish the interfacial gap states. The DOSs of GaN and HfO_2 bulk atoms (far from the interface) are given as a reference to identify the VBMs. The origin of the interface states is revealed in section 3.5.

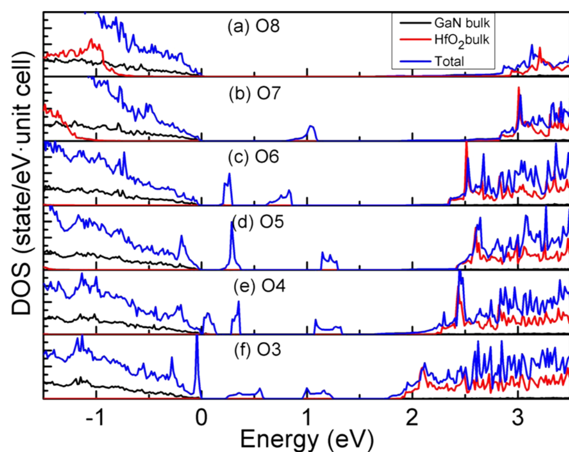

Figure 7. (a−f) Density of states for interfaces O8−O3, respectively. The black, red, and blue lines represent the GaN bulk, HfO_2 bulk, and normalized interface total DOS, respectively. The VBMs are aligned at 0.

The electronic structure indicates that no interface states are present in the O8 model (Figure 7(a)), establishing a high quality interface. Thus, cubic GaN can serve as an interlayer material at the interfacial structure between GaAs and high-*k* dielectrics. Nevertheless, interfacial states emerge when the interfacial oxygen content decreases (Figure 7(b−f)), which means that the oxygen-poor condition introduces interface states, leading to Fermi level pinning and degraded device performance. For situations in which oxygen vacancies exist (Figure 8(a−c)), pinning takes place.

3.5. Origins of Interface States.

As discussed above, III−V/dielectric interfaces have high density interface states, leading to poor device performance. Thus, we elucidated the origin of the interface states by local density of states (LDOS) analysis with the goal of determining a way to reduce the interface states. Figure 9 shows the LDOS of each system, with the contribution of bulk GaN and HfO_2 atoms marked with black and red lines, respectively, which was used to locate the VBM and CBM in the interfacial structure. The VBMs are aligned at 0 to distinguish the interfacial gap states. The LDOS of atoms that donate to the gap states are also marked.

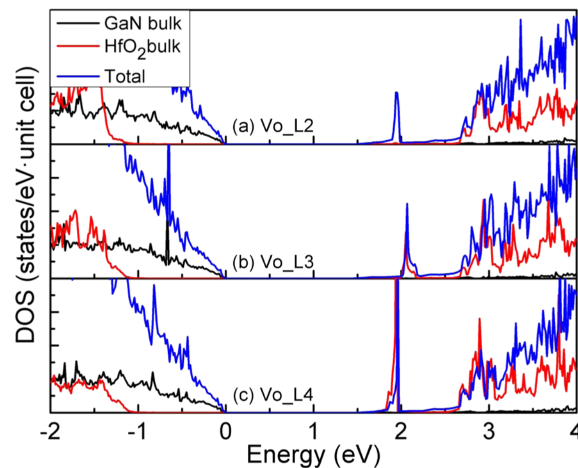

Figure 8. (a−c) Density of states for interfaces Vo_L2−Vo_L4, respectively. The black, red, and blue lines represent the GaN bulk, HfO_2 bulk, and normalized interface total DOS, respectively. The VBMs are aligned at 0.

First, we analyzed the O8 model. In Figure 7(a), it is clear that the O8 system shows a high quality interface. For O7, the removal of an interfacial O atom damages bonds at the interface. From the DOS displayed in Figure 7(b), there exists a flat band near the Fermi level (~1.06 eV), leading to Fermi level pinning. Figure 9(a) shows the LDOS of atoms contributing to the interface states in O7. The interface state density comes mainly from the contribution of two interfacial Ga atoms labeled as *Ga1* and *Ga2*, which are highlighted with dashed lines in Figure 9(a). Bader charge analysis[60] shows that the two Ga atoms have 1.79 and 1.96 electrons, respectively, which are more than that in Ga_2O_3 (1.40 e) but less than that in Ga_2O (2.48 e). Thus, the two Ga atoms are unsaturated.

From the DOS of the O6 model (Figure 7(c)), an interface state near the Fermi level at ~0.80 eV causes Fermi level pinning, and there is another strong gap state at a deeper energy level (~0.25 eV). Through analysis of the LDOS (Figure 9(b)), we found that the interface state of O6 is caused mainly by two parts: four Ga atoms at the interface and three N atoms connected to the Ga atoms. Two of the Ga atoms were discovered to contribute nearly equally and are marked as Ga1 and Ga2. Their co-contribution is termed Ga-type 1, and it is the primary cause of the Fermi level pinning (~0.80 eV). The Bader charges are 1.88 and 1.95 e, respectively. The other two Ga atoms, marked as Ga3 (1.99 e) and Ga4 (2.00 e), also have similar contributions, and their co-contribution is termed Ga-type 2. It can be seen from the LDOS that Ga-type 2 accounts for the origin of interface state near 0.25 eV. Moreover, the three N atoms (termed N1, N2, and N3) connected with the interfacial Ga atoms also contribute almost identically to the interface states, and their co-contributions are termed N-type 1 and are displayed in Figure 9(b).

As the interfacial oxygen content decreases, the origin of interface state for O5 becomes more complex. We can find that there are two interface states in O5 (Figure 7(d)), one near the Fermi level (~1.25 eV) and the other at ~0.30 eV. According

DOI: 10.1021/am507287f
ACS Appl. Mater. Interfaces 2015, 7, 5141−5149

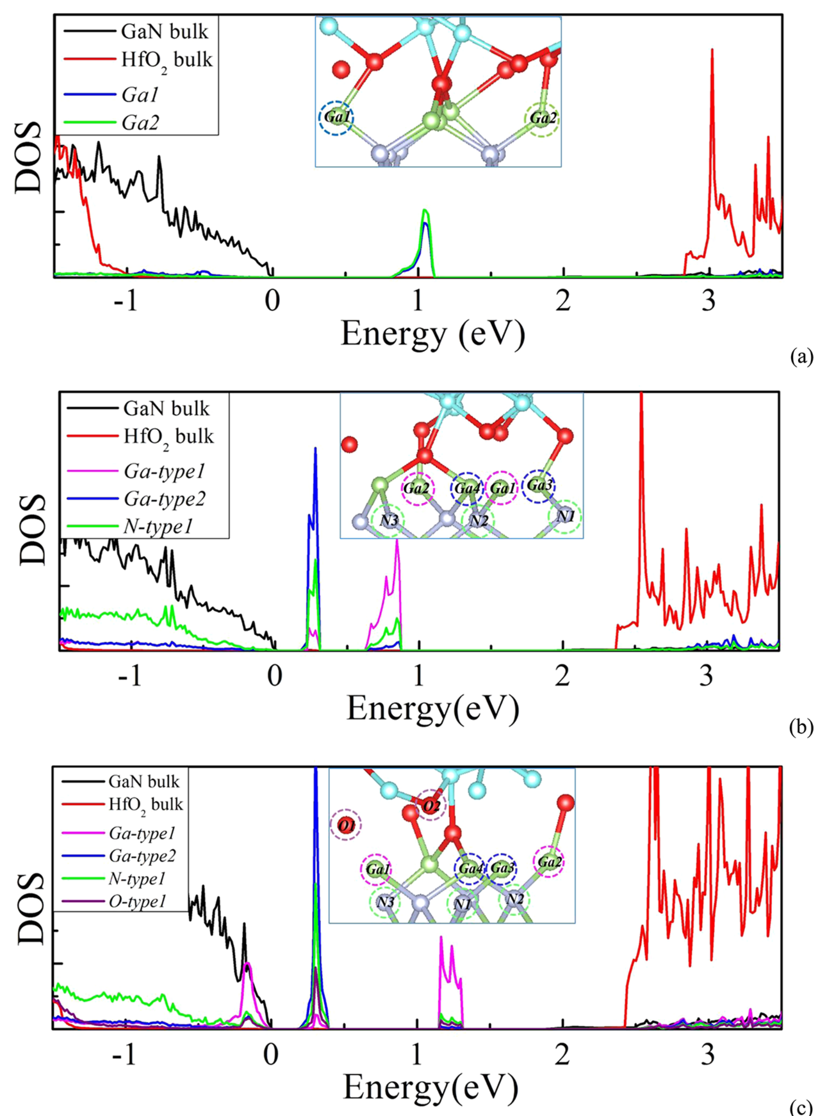

Figure 9. Local density of states of atoms contributing to the interface states in (a) O7, (b) O6, and (c) O5. The LDOS of bulk GaN and HfO_2 atoms are marked with black and red lines, respectively. The VBMs are aligned at 0.

Table 3. Bader Charges of Atoms Contributing to the Interface States

model	Ga1	Ga2	Ga3	Ga4	N1	N2	N3	O1	O2
O7	1.7907	1.9674							
O6	1.8842	1.9519	1.991	1.9967	6.3756	6.3769	6.3652		
O5	2.5319	1.9831	2.0230	1.9752	6.3790	6.3816	6.3749	7.1619	7.1164

to the LDOS in Figure 9(c), the origins of O5′s interface states contain four Ga atoms, three N atoms, and two O atoms at the interface. The Bader charges of each of the atoms are listed in Table 3.

With a further decrease of the interfacial oxygen content, the interfacial structure changes dramatically with more atoms contributing to the interface states. Furthermore, when the interfacial O atom content falls below 50% (less than 5 O atoms at the interface), the conduction band offset is too small thereby nullifying the need for deeper investigation.

4. CONCLUSION

In conclusion, cubic HfO_2/GaN interfaces were investigated by first-principles calculations. The theoretical results show that GaN is a promising interfacial layer to improve III−V/high-*k* interfaces used in high mobility devices. With decreasing interfacial oxygen contents, the bond length of the interfacial Ga−O bond changes. The O8 model presents the most stability from an O-rich environment. By reducing the interfacial O contents from 100 to 25% (i.e., varying the oxygen partial pressure during oxide growth), we find that the interface formation energy increases from −0.67 to −0.22 eV. The interfaces become more unstable when sublayer oxygen vacancies exist compared to that of the ideal interface (O8). The valence band offset changes from 0.51 to 1.97 eV with the decline of interfacial O contents. Specifically, the VBO of the O8 model (0.51 eV) indicates a practical GaAs/GaN/HfO_2 sandwich structure. Further work on the electronic structures shows that the O8 model establishes a high quality interface

DOI: 10.1021/am507287f
ACS Appl. Mater. Interfaces 2015, 7, 5141−5149

without gap states. Thus, GaN can serve as a passivation layer to avoid the formation of gap states between GaAs and HfO_2. Nevertheless, a significant interface state density emerges when the interfacial oxygen content decreases or an oxygen vacancy exists. The interface states, leading to Fermi level pinning, originate from two unsaturated interfacial Ga atoms based on the local density of states (LDOS) and Bader charge analyses. These results imply that the GaN/HfO_2 interface can present useful characteristics and provide a passivation layer for III−V MOS device technology.

■ ASSOCIATED CONTENT

Ⓢ Supporting Information

Properties of cubic GaN bulk and surface reconstructions, slab rotation details of lattice mismatch of GaN/GaAs interfaces, surface layer thickness testing, and initial movement testing details. This material is available free of charge via the Internet at http://pubs.acs.org.

■ AUTHOR INFORMATION

Corresponding Author

*E-mail: weichaowang@nankai.edu.cn.

Notes

The authors declare no competing financial interest.

■ ACKNOWLEDGMENTS

This work is supported by the National Natural Science Foundation of China (11304161, 11104148, and 51171082), Tianjin Natural Science Foundation (13JCYBJC41100 and 14JCZDJC37700), the National Basic Research Program of China (973 Program with 2014CB931703), Specialized Research Fund for the Doctoral Program of Higher Education (20110031110034), and the Fundamental Research Funds for the Central Universities. We thank the technology support from the Texas Advanced Computing Center (TACC) at the University of Texas at Austin (http://www.tacc.utexas.edu) for providing grid resources that have contributed to the research results reported within this paper. We thank Prof. Yoshio Nishi (Stanford) for inspiration and useful discussions.

■ REFERENCES

(1) Ferain, I.; Colinge, C. A.; Colinge, J. P. Multigate Transistors as the Future of Classical Metal−Oxide−Semiconductor Field-Effect Transistors. *Nature* **2011**, *479*, 310−316.

(2) del Alamo, J. A. Nanometre-Scale Electronics with III−V Compound Semiconductors. *Nature* **2011**, *479*, 317−323.

(3) Chau, R.; Doyle, B.; Datta, S.; Kavalieros, J.; Zhang, K. Integrated Nanoelectronics for the Future. *Nat. Mater.* **2007**, *6*, 810−812.

(4) He, G.; Zhu, L.; Sun, Z.; Wan, Q.; Zhang, L. Integrations and Challenges of Novel High-*k* Gate Stacks in Advanced CMOS Technology. *Prog. Mater. Sci.* **2011**, *56*, 475−572.

(5) Wilk, G. D.; Wallace, R. M.; Anthony, J. M. High-Gate Dielectrics: Current Status and Materials Properties Considerations. *J. Appl. Phys.* **2011**, *89*, 5243−5275.

(6) Lin, H. C.; Ye, P. D.; Wilk, G. D. Leakage Current and Breakdown Electric-Field Studies on Ultrathin Atomic-Layer-Deposited Al_2O_3 on GaAs. *Appl. Phys. Lett.* **2005**, *87*, 182904−182906.

(7) Chen, P. T.; Sun, Y.; Kim, E.; McIntyre, P. C.; Tsai, W.; Garner, M.; Pianetta, P.; Nishi, Y.; Chui, C. O. HfO_2 Gate Dielectric on $(NH_4)_2S$ Passivated (100) GaAs Grown by Atomic Layer Deposition. *J. Appl. Phys.* **2008**, *103*, 034106/1−034106/6.

(8) Jin, D.; Kim, D.; Kim, T.; del Alamo, J. A. Quantum Capacitance in Scaled Down III-V FETs. *IEEE Int. Electron Devices Meet.* **2009**, 495−498.

(9) Lin, L.; Robertson, J. Defect States at III-V Semiconductor Oxide Interfaces. *Appl. Phys. Lett.* **2011**, *98*, 082903/1−082903/3.

(10) Passlack, M.; Droopad, R.; Brammertz, G. Suitability Study of Oxide/Gallium Arsenide Interfaces for MOSFET Applications. *IEEE Trans. Electron Devices* **2010**, *57*, 2944−2956.

(11) Galatage, R. V.; Zhernokletov, D. M.; Dong, H.; Brennan, B.; Hinkle, C. L.; Wallace, R. M.; Vogel, E. M. Accumulation Capacitance Frequency Dispersion of III-V Metal-Insulator-Semiconductor Devices due to Disorder Induced Gap States. *J. Appl. Phys.* **2014**, *116*, 014504/1−014504/9.

(12) Hinkle, C. L.; Milojevic, M.; Brennan, B.; Sonnet, A. M.; Aguirre-Tostado, F. S.; Hughes, G. J.; Vogel, E. M.; Wallace, R. M. Detection of Ga Suboxides and Their Impact on III-V Passivation and Fermi-level Pinning. *Appl. Phys. Lett.* **2009**, *94*, 162101/1−162101/3.

(13) Oktyabrsky, S.; Ye, P. D., Eds. *Fundamentals of III-V Semiconductor MOSFETs*; Springer: New York, 2010.

(14) Agrawal, B. K.; Agrawal, S.; Srivastava, R. First-Principles Calculation of Valence Band Offset and the Interface States in GaAs/GaN(001) Superlattice. *Surf. Sci.* **1999**, *424*, 232−243.

(15) Strite, S.; Ruan, J.; Li, Z.; Salvador, A.; Chen, H.; Smith, D. J.; Choyke, W. J.; Morkoç, H. An Investigation of the Properties of Cubic GaN Grown on GaAs by Plasma-Assisted Molecular-Beam Epitaxy. *J. Vac. Sci. Technol., B: Microelectron. Nanometer Struct.* **1991**, *9*, 1924−1929.

(16) Goldman, R. S.; Feenstra, R. M.; Briner, B. G.; O'Steen, M. L.; Hauenstein, R. J. Atomic Scale Structure and Electronic Properties of GaN/GaAs Superlattices. *Appl. Phys. Lett.* **1996**, *69*, 3698−3700.

(17) Sonnet, A. M.; Galatage, R. V.; Hurley, P. K.; Pelucchi, E.; Thomas, K.; Gocalinska, A.; Huang, J.; Goel, N.; Bersuker, G.; Kirk, W. P.; Hinkle, C. L.; Vogel, E. M. Remote Phonon and Surface Roughness Limited Universal Electron Mobility of $In_{0.53}Ga_{0.47}As$ Surface Channel MOSFETs. *Microelectron. Eng.* **2011**, *88*, 1083−1086.

(18) Guo, Y.; Lin, L.; Robertson, J. Nitrogen Passivation at $GaAs:Al_2O_3$ Interfaces. *Appl. Phys. Lett.* **2013**, *102*, 091606/1−091606/3.

(19) Cabrera, W.; Brennan, B.; Dong, H.; O'Regan, T. P.; Povey, I. M.; Monaghan, S.; O'Connor, E.; Hurley, P. K.; Wallace, R. M.; Chabal, Y. J. Diffusion of $In_{0.53}Ga_{0.47}As$ Elements Through Hafnium Oxide During Post Deposition Annealing. *Appl. Phys. Lett.* **2014**, *104*, 011601/1−011601/5.

(20) Krylov, I.; Gavrilov, A.; Eizenberg, M.; Ritter, D. Indium Out Diffusion and Leakage Degradation in $Metal/Al_2O_3/In_{0.53}Ga_{0.47}As$ Capacitors. *Appl. Phys. Lett.* **2013**, *103*, 053502/1−053502/3.

(21) Hong, C. H.; Pavlidis, D.; Brown, S. W.; Rand, S. C. Photoluminescence Investigation of GaN Films Grown by Metal Organic Chemical Vapor Deposition on (100) GaAs. *J. Appl. Phys.* **1995**, *77*, 1705−1709.

(22) Yang, H.; Brandt, O.; Ploog, K. MBE Growth of Cubic GaN on GaAs Substrates. *Phys. Status Solidi B* **1996**, *194*, 109−120.

(23) Yoshida, S.; Okumura, H.; Misawa, S.; Sakuma, E. Hetero-Epitaxial Growth of Cubic GaN on GaAs by Gas-Source Molecular Beam Epitaxy. *Surf. Sci.* **1992**, *267*, 50−53.

(24) Zheng, X. H.; Wang, Y. T.; Feng, Z. H.; Yang, H.; Chen, H.; Zhou, J. M.; Liang, J. W. Method for Measurement of Lattice Parameter of Cubic GaN Layers on GaAs (001). *J. Cryst. Growth* **2003**, *250*, 345−348.

(25) Amimer, K.; Georgakilas, A.; Tsagaraki, K.; Androulidaki, M.; Cengher, D.; Toth, L.; Pecz, B.; Calamiotou, M. Single-Crystal Hexagonal and Cubic GaN Growth Directly on Vicinal (001) GaAs Substrates by Molecular-Beam Epitaxy. *Appl. Phys. Lett.* **2000**, *76*, 2580−2582.

(26) Kudrawiec, R.; Tschumak, E.; Misiewicz, J.; As, D. J. Contactless Electroreflectance Study of Fermi-level Pinning at the Surface of Cubic GaN. *Appl. Phys. Lett.* **2010**, *96*, 241904/1−241904/3.

(27) Cook, T. E., Jr.; Fulton, C. C.; Mecouch, W. J.; Davis, R. F.; Lucovsky, G.; Nemanich, R. J. Band Offset Measurements of the GaN (0001)/HfO_2 Interface. *J. Appl. Phys.* **2003**, *94*, 7155−7158.

DOI: 10.1021/am507287f
ACS Appl. Mater. Interfaces 2015, 7, 5141−5149

(28) Braun, S.; Salaneck, W. R.; Fahlman, M. Energy-Level Alignment at Organic/Metal and Organic/Organic Interfaces. *Adv. Mater.* **2009**, *21*, 1450−1472.
(29) Chen, L.; Ludeke, R.; Cui, X. D.; Schrott, A. G.; Kagan, C. R.; Brus, L. E. Electrostatic Field and Partial Fermi Level Pinning at the Pentacene-SiO_2 Interface. *J. Phys. Chem. B* **2005**, *109*, 1834−1838.
(30) Guo, Y.; Lin, L.; Robertson, J. Nitrogen passivation at GaAs:Al_2O_3 Interfaces. *Appl. Phys. Lett.* **2013**, *102*, 091606/1−091606/4.
(31) Chobpattana, V.; Son, J.; Law, J. M.; Engel-Herbert, R.; Huang, C.; Stemmer, S. Nitrogen-Passivated Dielectric/InGaAs Interfaces with Sub-nm Equivalent Oxide Thickness and Low Interface Trap Densities. *Appl. Phys. Lett.* **2013**, *102*, 022907/1−022907/3.
(32) Wheeler, D.; Wernersson, L. E.; Fröberg, L.; Thelander, C.; Mikkelsen, A.; Weststrate, K. J.; Sonnet, A.; Vogel, E. M.; Seabaugh, A. Deposition of HfO_2 on InAs by Atomic-Layer Deposition. *Microelectron. Eng.* **2009**, *86*, 1561−1563.
(33) Hohenberg, P.; Kohn, W. Inhomogeneous Electron Gas. *Phys. Rev.* **1964**, *136*, 864−871.
(34) Kohn, W.; Sham, L. J. Self-Consistent Equations Including Exchange and Correlation Effects. *Phys. Rev.* **1965**, *140*, 1133−1138.
(35) Perdew, J. P.; Burke, K.; Ernzerhof, M. Generalized Gradient Approximation Made Simple. *Phys. Rev. Lett.* **1996**, *77*, 3865−3868.
(36) Kresse, G.; Furthmüller, J. Efficient Iterative Schemes for *ab initio* Total-Energy Calculations Using a Plane-Wave Basis Set. *Phys. Rev. B* **1996**, *54*, 11169−11186.
(37) Kresse, G.; Furthmüller, J. Efficiency of ab Initio Total Energy Calculations for Metals and Semiconductors Using a Plane-Wave Basis Set. *Comput. Mater. Sci.* **1996**, *6*, 15−50.
(38) Blöchl, P. E. Projector Augmented Wave Method. *Phys. Rev. B* **1994**, *50*, 17953−17979.
(39) Chang, Y. C.; Huang, M. L.; Chang, Y. H.; Lee, Y. J.; Chiu, H. C.; Kwo, J.; Hong, M. Atomic-Layer-Deposited Al_2O_3 and HfO_2 on GaN: A Comparative Study on Interfaces and Electrical Characteristics. *Microelectron. Eng.* **2011**, *88*, 1207−1210.
(40) Chang, Y. C.; Chiu, H. C.; Lee, Y. J.; Huang, M. L.; Lee, K. Y.; Hong, M.; Chiu, Y. N.; Kwo, J.; Wang, Y. H. Structural and Electrical Characteristics of Atomic Layer Deposited High HfO_2 on GaN. *Appl. Phys. Lett.* **2007**, *90*, 232904/1−232904/3.
(41) Zhu, J.; Liu, Z. G. Structure and Dielectric Properties of Ultra-Thin ZrO_2 Films for High-*k* gate Dielectric Application Prepared by Pulsed Laser Deposition. *Appl. Phys. A: Mater. Sci. Process.* **2004**, *78*, 741.
(42) Press, W. H; Flannery, B. P.; Teukolsky, S. A.; Vetterling, W. T. *Numerical Recipes*; Cambridge University Press: New York, 1986.
(43) Bonilla, R. S.; Reichel, C.; Hermle, M.; Wilshaw, P. R. On the Location and Stability of Charge in SiO_2/SiNx Dielectric Double Layers Used for Silicon Surface Passivation. *J. Appl. Phys.* **2014**, *115* (14), 144105/1−144105/8.
(44) Benner, F.; Jordan, P. M.; Richter, C.; Simon, D. K.; Dirnstorfer, I.; Knaut, M.; Bartha, J. W.; Mikolajick, T. Atomic Layer Deposited High-Nanolaminates for Silicon Surface Passivation. *J. Vac. Sci. Technol., B: Nanotechnol. Microelectron.* **2014**, *32*, 03D110/1−03D110/6.
(45) Zhao, Z.; Zhang, B.; Li, P.; Guo, W.; Liu, A. Effective Passivation of Large Area Black Silicon Solar Cells by SiO_2/SiNx: Stacks. *Int. J. Photoenergy* **2014**, *2014*, 683654/1−683654/6.
(46) Lide R. D., Ed. *CRC Handbook of Chemistry and Physics*, 87th ed. (internet version); 2007; p 9−77.
(47) Wang, W.; Xiong, K.; Wallace, R. M.; Cho, K. Impact of Interfacial Oxygen Content on Bonding, Stability, Band Offsets, and Interface States of GaAs:HfO_2 Interfaces. *J. Phys. Chem. C* **2010**, *114*, 22610−22618.
(48) Yoshioka, S.; Hayashi, H.; Kuwabara, A.; Oba, F.; Matsunaga, K.; Tanaka, I. Structures and Energetics of Ga_2O_3 Polymorphs. *J. Phys.: Condens. Matter* **2007**, *19*, 346211/1−346211/11.
(49) Roy, R.; Hill, V. G.; Osborn, E. F. Polymorphism of Ga_2O_3 and the System Ga_2O_3-H_2O. *J. Am. Chem. Soc.* **1952**, *74*, 719−722.
(50) Finnis, M. W.; Lozovoi, A. Y.; Alavi, A. The Oxidation of NiAl: What Can We Learn from Ab Initio Calculations? *Annu. Rev. Mater. Res.* **2005**, *35*, 167−207.
(51) Monaghan, S.; Greer, J. C.; Elliott, S. D. Atomic Scale Model Interfaces between High-*k* Hafnium Silicates and Silicon. *Phys. Rev. B* **2007**, *75*, 245304/1−245304/14.
(52) Robertson, J. Band Offsets of Wide-Band-Gap Oxides and Implications for Future Electronic Devices. *J. Vac. Sci. Technol. B* **2000**, *18*, 1785−1791.
(53) Bass, J. M.; Oloumi, M.; Matthai, C. C. A Method for Determining Band Offsets in Semiconductor Superlattices and Interfaces. *J. Phys.: Condens. Matter* **1989**, *1*, 10625−10628.
(54) Lei, T.; Moustakas, T. D.; Graham, R. J.; He, Y.; Berkowitz, S. J. Epitaxial Growth and Characterization of Zinc Blende Gallium Nitride on (001) Silicon. *J. Appl. Phys.* **1992**, *71*, 4933−4943.
(55) Powell, R. C.; Lee, N. E.; Kim, Y. W.; Greene, J. E. Heteroepitaxial Wurtzite and Zinc Blende Structure GaN Grown by Reactiveion Molecular Beam Epitaxy: Growth Kinetics, Microstructure, and Properties. *J. Appl. Phys.* **1993**, *73*, 189−204.
(56) Coan, M. R.; Woo, J. H.; Johnson, D.; Gatabi, I. R.; Harris, H. R. Band Offset Measurements of the GaN/Dielectric Interfaces. *J. Appl. Phys.* **2012**, *112*, 024508/1−024508/6.
(57) Van de Walle, C. G.; Martin, R. M. Theoretical Study of Band Offsets at Semiconductor Interfaces. *Phys. Rev. B* **1987**, *35*, 8154−8165.
(58) Al-Allak, H. M.; Clark, S. J. Valence-Band Offset of the Lattice-Matched β-$FeSi_2$ (100)/Si(001) Heterostructure. *Phys. Rev. B* **2001**, *63*, 033311/1−033311/4.
(59) Robertson, J. High Dielectric Constant Gate Oxides for Metal Oxide Si Transistors. *Rep. Prog. Phys.* **2006**, *69*, 327−396.
(60) Henkelman, G.; Arnaldsson, A.; Jònsson, H. A Fast and Robust Algorithm for Bader Decomposition of Charge Density. *Comput. Mater. Sci.* **2006**, *36*, 354−360.

DOI: 10.1021/am507287f
ACS Appl. Mater. Interfaces 2015, 7, 5141−5149